

## Independent Operation of Two Waveguide-Integrated Quantum Emitters

C. Papon<sup>1,\*</sup>, Y. Wang,<sup>1</sup> R. Uppu,<sup>1,†</sup> S. Scholz,<sup>2</sup> A.D. Wieck<sup>1,2</sup>, A. Ludwig<sup>1,2</sup>, P. Lodahl,<sup>1</sup> and L. Midolo<sup>1</sup>

<sup>1</sup>Center for Hybrid Quantum Networks (*Hy-Q*), The Niels Bohr Institute, University of Copenhagen, Copenhagen Ø DK-2100, Denmark

<sup>2</sup>Lehrstuhl für Angewandte Festkörperphysik, Ruhr-Universität Bochum, Universitätsstraße 150, Bochum 44801, Germany

(Received 14 October 2022; revised 11 April 2023; accepted 1 May 2023; published 27 June 2023)

We demonstrate the resonant excitation of two quantum dots in a photonic integrated circuit for on-chip single-photon generation in multiple spatial modes. The two quantum dots are electrically tuned to the same emission wavelength using a pair of isolated *p-i-n* junctions and excited by a resonant pump laser via dual-mode waveguides. We demonstrate two-photon quantum interference visibility of  $(79 \pm 2)\%$  under continuous-wave excitation of narrow-linewidth quantum dots. Our work solves an outstanding challenge in quantum photonics by realizing the key enabling functionality of how to scale up deterministic single-photon sources.

DOI: 10.1103/PhysRevApplied.19.L061003

The coherent generation and manipulation of single photons using solid-state quantum emitters are key resources for the development of scalable quantum information protocols [1] to realize quantum simulators [2,3] or quantum communication hardware [4–6]. Significant progress has been made with InAs self-assembled quantum dots (QDs) embedded in GaAs photonic nanostructures [7], where ultrahigh-quality epitaxial growth [8] combined with reproducible low-electrical-noise photonic devices enables highly coherent photon emission [9–11] and near-transform-limited spectral linewidths [12,13]. Embedding QDs in thin membranes further enables direct integration of single-photon sources (SPSs) in waveguides, resulting in near-unity light-matter interaction and deterministic source operation, with streams of hundreds of indistinguishable photons being generated [10].

The scalability of the QD platform has previously been demonstrated by interfering photons from remote emitters in distant cryostats [14–16]. However, the scalable control and operation of waveguide-coupled quantum emitters within the same photonic integrated circuit have not been reported yet (see Ref. [17] for a comparison with

Refs. [14–16,18–20]). A major roadblock has been the lack of control over the spectral and spatial distribution of self-assembled QDs [21], together with the absence of a strategy for addressing several QDs simultaneously. For these reasons, most multiphoton experiments have relied on spatiotemporal demultiplexing of a single quantum emitter [22–24], for which full on-chip integration is highly challenging. Alternatively, the dc Stark effect [25] may be employed as the tuning mechanism mitigating the effect of inhomogeneous broadening for the integration of multiple QDs [26] in the same photonic circuit. Recently, an SPS was demonstrated using a dual-mode waveguide, whose operational principle exploits one mode for excitation of QDs and the second mode for collection of single photons [27]. With this method, a single resonant laser may be distributed on-chip to excite multiple waveguide-integrated quantum emitters [see Fig. 1(a)], thus offering a route to large-scale integration, ultimately enabling on-chip quantum information protocols.

In the present letter, we demonstrate the independent operation of two quantum emitters using a tailored nanophotonic circuit, whose design principle can be further scaled to a larger number of emitters. We realize simultaneous resonant excitation of two QDs positioned in separate dual-mode waveguides and demonstrate their independent Stark tuning with electrical biases applied locally. The device is based on a *p-i-n* GaAs membrane containing QDs in its center and individual frequency tuning is implemented by fabricating local electrical contacts. A polarization diversity grating (PDG) [28] allows distributing the same excitation laser to the individual waveguides and equalizing the Rabi frequency of each QD in units of their respective decay rate. The single-photon

\*cpapon@mit.edu

<sup>†</sup>Present address: Department of Physics and Astronomy, University of Iowa, 205 N. Madison Street, Iowa City, Iowa 52242, USA.

Published by the American Physical Society under the terms of the [Creative Commons Attribution 4.0 International license](#). Further distribution of this work must maintain attribution to the author(s) and the published article's title, journal citation, and DOI.

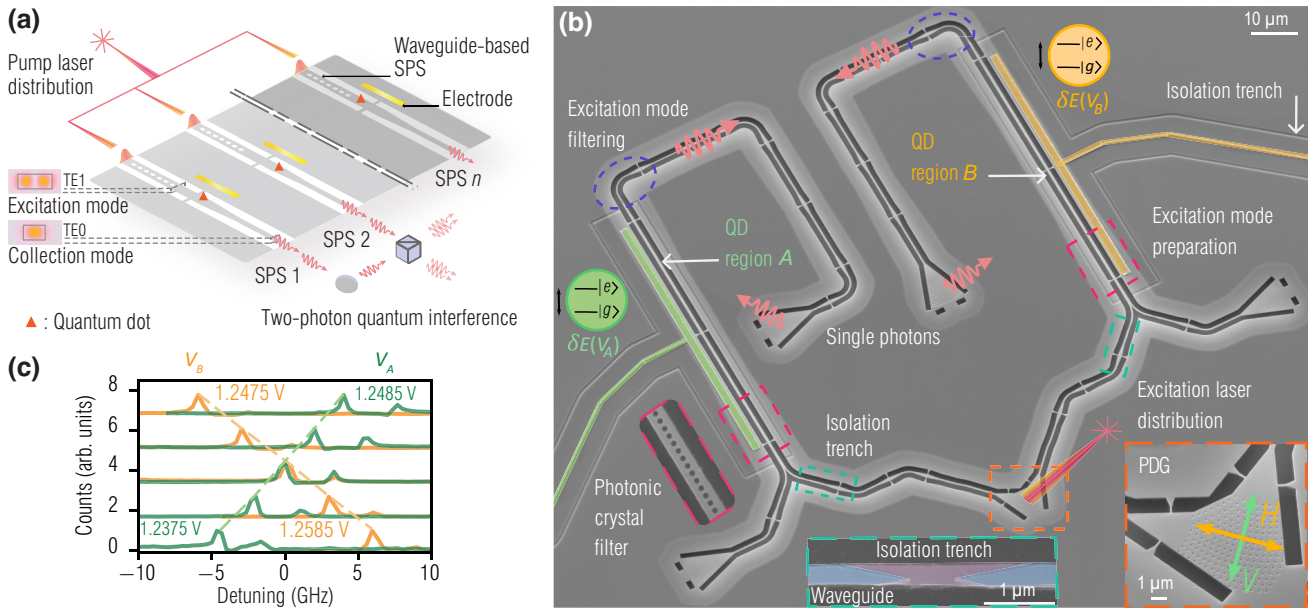


FIG. 1. (a) Sketch of a fully waveguide-integrated scheme for generating single photons in multiple spatial modes, where a single laser source is distributed on-chip (not shown) to  $n$  waveguide-based SPSs. Resonant excitation is performed by a dual-mode waveguide geometry where excitation occurs through the TE1 mode and pump is removed by tapering the waveguide after the QD. Collection of single photons is done via the TE0 waveguide mode. Independent electrical tuning of the QDs accounts for spectral inhomogeneities. (b) SEM of the actual device designed for  $n = 2$ . A monochromatic laser is coupled through a PDG (orange dashed area and inset) and is prepared in the mode for resonant excitation by the dual-mode waveguide and the photonic crystal filter (red dashed area and inset). QDs are simultaneously excited in regions  $A$  and  $B$  and are independently biased using two electrodes (green and orange shadow, respectively), isolated by shallow-etched trenches (blue dashed area and inset, purple shadow) on the waveguides (blue shadow) to isolate the  $p$  layer of the two QD regions. (c) Resonance fluorescence of two QDs,  $QD_A$  and  $QD_B$ , obtained by sweeping  $V_A$  (green curve) and  $V_B$  (orange curve), excited with a resonant laser locked at 320.705 THz. Counts are normalized by the peak value of each QD and shifted for clarity.

character of the emission is analyzed from second-order correlation measurements of each QD under continuous-wave (cw) resonant excitation. Finally, two-photon quantum interference (TPQI) between two independently controlled QDs is realized, which is a key result demonstrating the scalability of the platform to multiple emitters.

A scanning electron microscope (SEM) image of the device is presented in Fig. 1(b). The footprint is only  $100 \times 125 \mu\text{m}^2$ , providing a compact building block, adoptable to larger number of resonant QDs. The entire structure has been fabricated on gated GaAs membranes (see the supplementary material of Ref. [27] for details) with a QD density of  $10 \mu\text{m}^{-2}$ , ensuring a high probability of finding two QDs Stark-tunable into mutual resonance [17]. A monochromatic laser is coupled to the device via a PDG [orange dashed area in Fig. 1(b)] distributing optical power into two entrance waveguides, with a ratio controlled with the incident light's polarization. The PDG, inspired from Ref. [28], has been entirely redesigned and optimized to operate at 930 nm on suspended GaAs waveguides [17]. The laser is initially prepared in a superposition of the fundamental (even-symmetry) and first-order (odd-symmetry) modes of a dual-mode waveguide by an inverted Y splitter and then

filtered by a one-dimensional photonic crystal mirror [inset of the red dashed area in Fig. 1(b)] so that only the odd mode reaches the QD regions [27]. The single photons are collected into the fundamental TE0 mode of the waveguide and routed towards the out-coupling shallow-etched grating [29], while the photonic crystal sections back-reflect any photons emitted towards the excitation port. The excitation laser is filtered by the first  $90^\circ$  bend [dashed purple circle in Fig. 1(b)], where the waveguide is adiabatically tapered. Independent Stark tuning of QDs in each waveguide is achieved by applying a homogeneous vertical electric field using electrodes (highlighted in orange and green) contacted to the  $p$  layer of the heterostructure. A global  $n$  back-contact is fabricated in the periphery of the structures. A set of 50-nm-deep isolation trenches surrounding the electrodes and crossing the waveguides [see blue dashed areas in Fig. 1(b)], previously reported for reducing the  $p-i-n$  diode capacitance and response time [12,30], have been adapted to the composite dual-mode waveguides device, to achieve isolated tuning of the two QD regions. The tapered geometry of the trenches ensures minimal optical losses.

The device is characterized at cryogenic temperature ( $T = 1.6 \text{ K}$ ) by coupling a cw laser through the PDG and

sweeping the bias voltage over the two QD regions. The resonance fluorescence (RF) collected from QD regions  $A$  and  $B$  is detected with two superconducting nanowire single-photon detectors (SNSPDs). Figure 1(c) shows the RF signal as a function of the frequency detuning between two different QDs defined as QD <sub>$A$</sub>  (green curve) and QD <sub>$B$</sub>  (orange curve) for a laser frequency-locked at 320.705 THz. From the full frequency-voltage plateau lines [17] in the Coulomb blockade regime [31,32], we attribute these states to the QD neutral exciton. The two transitions are brought in mutual resonance by sweeping simultaneously  $V_A$  and  $V_B$ , the voltage on waveguide  $A$  and  $B$ , respectively, without crosstalk [17]. Both QDs have a weak second transition frequency-shifted by approximately 3 GHz, attributed to the second dipole of the neutral exciton [10], whose coupling efficiency to the waveguide depends on the QD lateral position [17,33–35].

The single-photon nature of the collected signal is confirmed by the measurement of the second-order correlation function,  $g^{(2)}(\tau)$ , shown in Fig. 2(a), at the voltages  $V_A$  and  $V_B$  ensuring mutual resonance between the two QDs. The time correlation between two SNSPDs is recorded for QD <sub>$A$</sub>  and QD <sub>$B$</sub> , and reveals a value at zero time delay of  $g_A^{(2)}(0) = 0.13 \pm 0.02$  (top) and  $g_B^{(2)}(0) = 0.04 \pm 0.02$  (bottom), respectively, limited by the finite laser suppression [17,36] sensitive to the fabrication reproducibility of the structure. Coincidence counts are normalized by the average value at long time delay and error bars are estimated from Poisson statistics. The  $g^{(2)}(\tau)$  functions are fitted [pink curves in Fig. 2(a)] with a model for resonant  $g^{(2)}(\tau)$  [37], which includes an exponential term accounting for the bunching observed at short time delay, [38] and the convolution with the instrument response function (IRF) of the SNSPDs. Radiative decay rates of  $\gamma_A = (1.46 \pm 0.03) \text{ ns}^{-1}$  and  $\gamma_B = (1.05 \pm 0.01) \text{ ns}^{-1}$  are extracted from the fit, for QD <sub>$A$</sub>  and QD <sub>$B$</sub> , respectively, after fixing the Rabi frequency to  $\Omega_A = 0.48\gamma_A$  and  $\Omega_B = 0.34\gamma_B$  from power saturation measurement [17,39]. By controlling the polarization of the incident laser on the PDG, we thus ensure similar driving conditions for each QD. We attribute the bunching at short time delay to the effect of spectral diffusion, visible in cross-correlation measurements with a narrow-bandwidth laser [40].

To further characterize the two QDs, time-resolved fluorescence under  $p$ -shell excitation through the waveguide is recorded, after spectral filtering of the fluorescence. The decay curves are shown in Fig. 2(b) and are fitted with a double exponential, where the fast decay rate is fixed to  $\gamma_A$  (QD <sub>$A$</sub> , left) and  $\gamma_B$  (QD <sub>$B$</sub> , right). For QD <sub>$A$</sub> , the presence of the second dipole is highlighted by the beating in the decay curve, with a fine structure splitting of  $\Delta_{\text{FSS}}/2\pi = 3.45 \pm 0.01$  GHz, in agreement with the RF spectra shown in Fig. 1(c). The fit also reveals a slow decay component attributed to the pronounced second dipole. Similarly, the fit of the decay curve of QD <sub>$B$</sub>  also

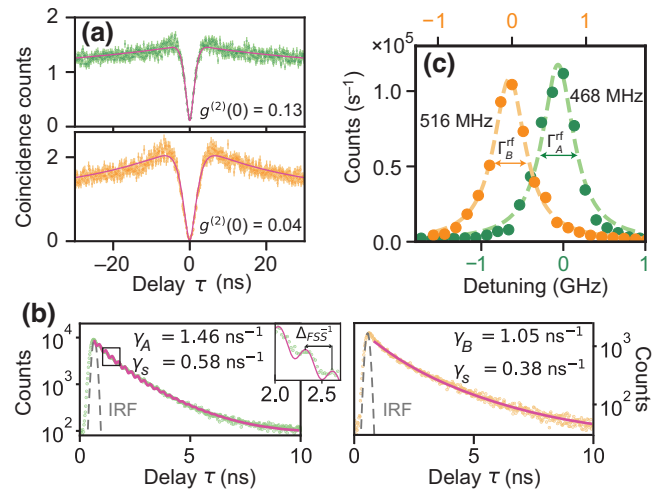


FIG. 2. (a) Second-order correlation functions of QD <sub>$A$</sub>  (top) and QD <sub>$B$</sub>  (bottom). The pink curves show the fit, from which we extract the radiative decay of each QD. (b) Lifetimes of QD <sub>$A$</sub>  (left) and QD <sub>$B$</sub>  (right) are recorded under  $p$ -shell excitation. The slow (fitted) and fast (fixed) decay rate of a double exponential (pink curves) is shown for both QDs. The fit to QD <sub>$A$</sub>  includes an oscillating term from the second dipole, with  $\Delta_{\text{FSS}}/2\pi = 3.45 \pm 0.01$  GHz. (c) RF scattered intensity as a function of laser detuning for QD <sub>$A$</sub>  (green dots) and QD <sub>$B$</sub>  (orange dots), below saturation. The dashed lines are the fits to a Lorentzian.

shows a slow component, which can be attributed to interaction with nonradiative states [41]. From the agreement between the measured decay curves and the model, we extract the lifetime-limited contribution to the linewidth of  $\Gamma_A = \gamma_A/2\pi = 233$  MHz and  $\Gamma_B = \gamma_B/2\pi = 167$  MHz for QD <sub>$A$</sub>  and QD <sub>$B$</sub> , respectively.

A fine-step RF scan of the two QDs excited simultaneously is shown in Fig. 2(c) and fitted with Lorentzian functions giving similar linewidths of  $\Gamma_A^{\text{RF}} = 468 \pm 28$  MHz and  $\Gamma_B^{\text{RF}} = 516 \pm 13$  MHz, for QD <sub>$A$</sub>  and QD <sub>$B$</sub> , respectively. Broadening beyond the transform limit ( $\Gamma_A$ ,  $\Gamma_B$ ) is attributed partly to power broadening [37] as highlighted in Ref. [17]. In the low-power limit, the linewidth of QD <sub>$A$</sub>  (QD <sub>$B$</sub> ) is  $1.2\Gamma_A$  ( $2.6\Gamma_B$ ), due to an additional contribution from slow spectral diffusion. This broadening is further characterized by fitting the low-power RF data to a Voigt function, thereby extracting the Gaussian distribution of spectral diffusion with standard deviation  $\sigma_A = 68 \pm 4$  MHz ( $\sigma_B = 163 \pm 25$  MHz) [17]. The effect of slow noise is comparable to previously recorded RF measurements on the same platform [10,27]. The electrically contacted sources have a twofold advantage: the individual tuning allows one to bring two different QDs on resonance, and the control of the charge environment reduces significantly the impact of charge noise [42], as observed from the narrow linewidths. Even narrower optical linewidths have previously been reported for the planar nanophotonic waveguide platform [12], which confirms the potential of the approach.

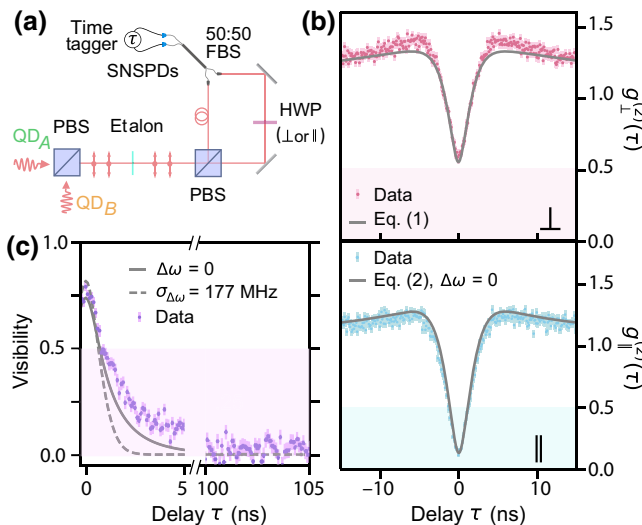


FIG. 3. (a) Schematic of the interferometer for TPQI measurements (FBS, fiber beam splitter; HWP, half-wave plate). (b) Top: Measured  $g_{\perp}^{(2)}(\tau)$  for cross-polarized photons (pink dots) with the prediction of Eq. (1) (gray curve). Bottom: Measured  $g_{\parallel}^{(2)}(\tau)$  for co-polarized photons (blue dots) with the prediction of Eq. (2) for  $\Delta\omega = 0$  (gray curve). The shaded regions indicate the thresholds below which nonclassical effects occur. (c) Visibility of the TPQI (purple dots). The plain (dashed) gray curve is the visibility calculated with  $\Delta\omega = 0$  (by averaging over a random distribution of width  $\sigma_{\Delta\omega} = 177$  MHz). The shaded region indicates the threshold above which nonclassical effects occur.

The low-noise characteristic of both resonant QDs enables testing TPQI. We perform a Hong-Ou-Mandel (HOM) experiment with a balanced Mach-Zender interferometer (MZI) under cw excitation [43], using the same excitation power condition as for the measurement of  $g^{(2)}(\tau)$ . The HOM setup is shown in Fig. 3(a). The photons collected from QD<sub>A</sub> and QD<sub>B</sub>, in orthogonally polarized modes, are combined on a polarized beam splitter (PBS) and spectrally filtered (3 GHz linewidth) to remove phonon sidebands [44] before entering the MZI. When the photons are orthogonally polarized, i.e., fully distinguishable, the probability  $g_{\perp}^{(2)}(\tau)$  of detecting photons on both detectors as a function of the time delay  $\tau$  between the two events is [20,45]

$$g_{\perp}^{(2)}(\tau) = c_A^2 g_A^{(2)}(\tau) + c_B^2 g_B^{(2)}(\tau) + 2c_A c_B, \quad (1)$$

where  $c_n = I_n/(I_A + I_B)$ ,  $I_n$  being the intensity recorded for QD<sub>n</sub> (for  $n \in \{A, B\}$ ), characterized over the HOM measurement to be, on average,  $c_A = 0.59$  and  $c_B = 0.41$ . The cross-polarized measurement is shown in Fig. 3(b) (pink dots, top) together with the prediction from Eq. (1) (gray curve) calculated with the fitted  $g_n^{(2)}(\tau)$  from Fig. 2(a).

TPQI is observed when both arms of the MZI have the same polarization, which results in a vanishing coincidence at small  $\tau$ . This measurement is shown in Fig. 3(b) (blue dots, bottom) with an observed TPQI dip

reduced much below the classical threshold of 0.5. The TPQI can be modeled with [20,45]

$$\begin{aligned} g_{\parallel}^{(2)}(\tau) &= c_A^2 g_A^{(2)}(\tau) + c_B^2 g_B^{(2)}(\tau) + 2R c_A c_B \\ &\times \left[ 1 - \zeta_A \zeta_B |g_A^{(1)}(\tau)| |g_B^{(1)}(\tau)| \cos(\Delta\omega\tau) \right], \end{aligned} \quad (2)$$

where  $R$  is a constant to ensure that  $\lim_{|\tau| \rightarrow \infty} g_{\parallel}^{(2)}(\tau) = 1$  [46] (see Ref. [17] for details). The residual laser photons account for imperfect interference through  $\zeta_n = \sqrt{1 - g_n^{(2)}(0)}$ . The first-order coherence function  $g_n^{(1)}(\tau)$  of QD<sub>n</sub> is a function of the lifetime of the emitters, Rabi frequency, and dephasing [47] and is calculated for this experiment with the measured parameters  $\gamma_A$ ,  $\gamma_B$ ,  $\Omega_A$ , and  $\Omega_B$  [17]. The dephasing rate is here neglected since it is not measured directly. Moreover, previous work in similar conditions shows that it contributes moderately to the loss of interference visibility [27]. For QDs fully resonant over the course of the experiment, we have  $\cos(\Delta\omega\tau) = 1$ , where  $\Delta\omega$  is the frequency detuning between the two emitters. The plain gray curve in Fig. 3(b) (bottom) is the expected  $g_{\parallel}^{(2)}(\tau)$  for  $\Delta\omega = 0$ , where only the normalization constant  $R$  is fitted [17,48]. The measured TPQI is well described by the model; however, the time response is slower than from calculation, indicating an overestimation of the decay rate and/or Rabi frequency. This can be corrected in the future by directly measuring the first-order coherence.

The visibility of the HOM measurement, defined as  $V(\tau) = 1 - g_{\parallel}^{(2)}(\tau)/g_{\perp}^{(2)}(\tau)$ , is displayed in Fig. 3(c) and reveals a raw peak of  $(79 \pm 2)\%$ , primarily limited by the nonzero  $g^{(2)}(0)$  of each QD. The visibility calculated with  $\Delta\omega = 0$  (plain gray curve) shows a significant overlap with the measured data, both in width, governed by the dynamics of the QDs, and in peak value, limited by the laser leakage measured in Fig. 2(a). Surprisingly, although low-power RF scans indicate the presence of slow spectral diffusion for both QDs, the TPQI dip and hence the visibility peak are well explained without taking this effect into account. To interpret this result, we calculate the visibility curve assuming that the spectral diffusion experienced by the two QDs is fully uncorrelated, meaning that the detuning  $\Delta\omega$  varies stochastically. In this case, the mutual detuning, on average  $\bar{\Delta\omega} = 0$ , would follow a normal distribution with  $\sigma_{\Delta\omega} = 177$  MHz, given by  $\sqrt{\sigma_A^2 + \sigma_B^2}$  [17], from which we perform an ensemble average of Eq. (2). We observe a clear deviation from this model in terms of the peak width, as shown in Fig. 3(c) (dashed gray curve), indicating that the dominant slow noise sources are not fully uncorrelated for independent QDs. This may be a result of the two QDs being biased by nearby electrodes, thereby featuring similar electrical-noise properties. We note that the calculated peak value of the visibility curves

differs due to the uncertainty added by the ensemble average and the normalization of the TPQI expression. The narrow bandwidth of the laser suppression from the current device prevented the implementation of triggered excitation with large signal-to-noise ratio, and hence the direct measurement of indistinguishability through the pulsed HOM experiment. Next-generation devices will focus on improving the performance of the laser filtering, in terms of bandwidth and fabrication imperfections.

In this letter, we showed the operational principle of a multi-QD photonic circuit for scaling up to multiple quantum emitters. We demonstrated the simultaneous resonant excitation of two QDs and their independent wavelength control. Laser suppression was achieved by the waveguide design and was confirmed by the measurement of strong antibunching in the second-order correlation function. We have analyzed two QDs in detail, both revealing narrow and similar emission linewidths showing the high coherence of the photon-emitter interface. We studied the presence of slow residual spectral diffusion and found that the effect on TPQI was limited due to correlated noise on the two QDs, i.e., the detrimental effect may be less severe than anticipated. It is also noted that residual slow noise can be further reduced by frequency-locking of the emitters [49]. Another route to improvement exploits Purcell enhancement by slow-light and dispersion engineering in a dual-mode photonic-crystal waveguide [50], as a direct extension of the present experiment. Furthermore, we showed that two quantum emitters can be conveniently controlled simultaneously, which, combined with pulsed excitation, represents the necessary hardware for coherent multi-emitter interaction [51] and device-independent quantum key distribution, requiring high source efficiency [5]. Moreover, scaling up to more sources could be realized by cascading a network of tunable beam splitters [52] for pump distribution, and tunable filters [53] could be integrated for phonon sideband suppression. This resonant excitation technique can also be adapted to different quantum emitter platforms, such as GaAs QDs, where high indistinguishability between remote QDs has been recently demonstrated [15].

Data and scripts are available upon request.

**Acknowledgments.**—We thank A. Tiranov for experimental assistance and E. M. González-Ruiz and A. S. Sørensen for guiding discussion on two-photon quantum interference. We thank Baptiste Karoubi for assistance in designing the concept figure. We gratefully acknowledge financial support from the Danish National Research Foundation (Center of Excellence Hy-Q DNRF139), Styrelsen for Forskning og Innovation (FI) (5072-00016B QUANTECH), Innovationsfonden (No. 9090-00031B, FIRE-Q), and the European Research Council (ERC) under the European Union’s Horizon 2020 research and innovation programme (Grant agreement No. 949043, NANOMEQ).

A.L., S.S., and A.D.W. acknowledge support of BMBF (QR.X Project 16KISQ009) and the DFG (383065199 and TRR 160/2-Project B04).

- [1] R. Uppu, *et al.*, Quantum-dot-based deterministic photon-emitter interfaces for scalable photonic quantum technology, *Nat. Nanotechnol.* **16**, 1308 (2021).
- [2] A. Peruzzo, *et al.*, A variational eigenvalue solver on a photonic quantum processor, *Nat. Commun.* **5**, 4213 (2014).
- [3] C. Sparrow, *et al.*, Simulating the vibrational quantum dynamics of molecules using photonics, *Nature* **557**, 660 (2018).
- [4] D. Buterakos, E. Barnes, and S. E. Economou, Deterministic Generation of All-Photonic Quantum Repeaters from Solid-State Emitters, *Phys. Rev. X* **7**, 041023 (2017).
- [5] E. M. González-Ruiz, S. K. Das, P. Lodahl, and A. S. Sørensen, Violation of Bell’s inequality with quantum-dot single-photon sources, *Phys. Rev. A* **106**, 012222 (2022).
- [6] J. Borregaard, *et al.*, One-Way Quantum Repeater Based on Near-Deterministic Photon-Emitter Interfaces, *Phys. Rev. X* **10**, 021071 (2020).
- [7] P. Lodahl, A. Ludwig, and R. J. Warburton, A deterministic source of single photons, *Phys. Today* **75**, 44 (2022).
- [8] N. Bart, *et al.*, Wafer-scale epitaxial modulation of quantum dot density, *Nat. Commun.* **13**, 1633 (2022).
- [9] G. Kiršanskė, *et al.*, Indistinguishable and efficient single photons from a quantum dot in a planar nanobeam waveguide, *Phys. Rev. B* **96**, 165306 (2017).
- [10] R. Uppu, *et al.*, Scalable integrated single-photon source, *Sci. Adv.* **6**, eabc8268 (2020).
- [11] N. Tomm, *et al.*, A bright and fast source of coherent single photons, *Nat. Nanotechnol.* **16**, 399 (2021).
- [12] F. T. Pedersen, Y. Wang, C. T. Olesen, S. Scholz, A. D. Wieck, A. Ludwig, M. C. Löbl, R. J. Warburton, L. Midolo, R. Uppu, and P. Lodahl, Near transform-limited quantum dot linewidths in a broadband photonic crystal waveguide, *ACS Photon.* **7**, 2343 (2020).
- [13] H. Ollivier, *et al.*, Reproducibility of high-performance quantum dot single-photon sources, *ACS. Photon.* **7**, 1050 (2020).
- [14] X. You, *et al.*, Quantum interference with independent single-photon sources over 300 km fiber, *Adv. Photon.* **4**, 066003 (2022).
- [15] L. Zhai, G. N. Nguyen, C. Spinnler, J. Ritzmann, M. C. Löbl, A. D. Wieck, A. Ludwig, A. Javadi, and R. J. Warburton, Quantum interference of identical photons from remote GaAs quantum dots, *Nat. Nanotechnol.* **17**, 829 (2022).
- [16] J. H. Weber, *et al.*, Two-photon interference in the telecom C-band after frequency conversion of photons from remote quantum emitters, *Nat. Nanotechnol.* **14**, 23 (2019).
- [17] See Supplemental Material at <http://link.aps.org/supplemental/10.1103/PhysRevApplied.19.L061003> for further device design information,  $\beta$ -factor calculation, further characterization of the resonance fluorescence of the two quantum dots, and a summary of previous work with two quantum dots.
- [18] D. J. P. Ellis, *et al.*, Independent indistinguishable quantum light sources on a reconfigurable photonic integrated circuit, *Appl. Phys. Lett.* **112**, 211104 (2018).

- [19] M. Reindl, K. D. Jöns, D. Huber, C. Schimpf, Y. Huo, V. Zwiller, A. Rastelli, and R. Trotta, Phonon-assisted two-photon interference from remote quantum emitters, *Nano Lett.* **17**, 4090 (2017).
- [20] R. B. Patel, A. J. Bennett, I. Farrer, C. A. Nicoll, D. A. Ritchie, and A. J. Shields, Two-photon interference of the emission from electrically tunable remote quantum dots, *Nat. Photon.* **4**, 632 (2010).
- [21] H. Vural, S. L. Portalupi, and P. Michler, Perspective of self-assembled InGaAs quantum-dots for multi-source quantum implementations, *Appl. Phys. Lett.* **117**, 030501 (2020).
- [22] F. Lenzini, *et al.*, Active demultiplexing of single photons from a solid-state source, *Laser Photon. Rev.* **11**, 1600297 (2017).
- [23] T. Hummel, C. Ouellet-Plamondon, E. Ugur, I. Kulkova, T. Lund-Hansen, M. A. Broome, R. Uppu, and P. Lodahl, Efficient demultiplexed single-photon source with a quantum dot coupled to a nanophotonic waveguide, *Appl. Phys. Lett.* **115**, 021102 (2019).
- [24] H. Wang, *et al.*, Boson Sampling with 20 Input Photons and a 60-Mode Interferometer in a  $10^{14}$ -Dimensional Hilbert Space, *Phys. Rev. Lett.* **123**, 250503 (2019).
- [25] R. J. Warburton, C. Schulhauser, D. Haft, C. Schäflein, K. Karrai, J. M. Garcia, W. Schoenfeld, and P. M. Petroff, Giant permanent dipole moments of excitons in semiconductor nanostructures, *Phys. Rev. B* **65**, 113303 (2002).
- [26] M. Petruzzella, *et al.*, Quantum photonic integrated circuits based on tunable dots and tunable cavities, *APL Photon.* **3**, 106103 (2018).
- [27] R. Uppu, *et al.*, On-chip deterministic operation of quantum dots in dual-mode waveguides for a plug-and-play single-photon source, *Nat. Commun.* **11**, 3782 (2020).
- [28] F. VanLaere, W. Bogaerts, P. Dumon, G. Roelkens, D. VanThourhout, and R. Baets, Focusing polarization diversity grating couplers in silicon-on-insulator, *J. Lightwave Technol.* **27**, 612 (2009).
- [29] X. Zhou, I. Kulkova, T. Lund-Hansen, S. L. Hansen, P. Lodahl, and L. Midolo, High-efficiency shallow-etched grating on GaAs membranes for quantum photonic applications, *Appl. Phys. Lett.* **113**, 251103 (2018).
- [30] M. H. Appel, *et al.*, Entangling a Hole Spin with a Time-Bin Photon: A Waveguide Approach for Quantum Dot Sources of Multiphoton Entanglement, *Phys. Rev. Lett.* **128**, 233602 (2022).
- [31] R. J. Warburton, Single spins in self-assembled quantum dots, *Nat. Mater.* **12**, 483 (2013).
- [32] J. Houel, *et al.*, Probing Single-Charge Fluctuations at a GaAs/AlAs Interface Using Laser Spectroscopy on a Nearby InGaAs Quantum Dot, *Phys. Rev. Lett.* **108**, 107401 (2012).
- [33] N. Rotenberg, P. Türschmann, H. R. Haakh, D. Martin-Cano, S. Götzinger, and V. Sandoghdar, Small slot waveguide rings for on-chip quantum optical circuits, *Opt. Express* **25**, 5397 (2017).
- [34] A. Taflove and S. Hagness, *Computational Electrodynamics: The Finite-Difference Time-Domain Method* (Artech, Norwood, MA, 2005).
- [35] A. F. Oskooi, D. Roundy, M. Ibanescu, P. Bermel, J. Joannopoulos, and S. G. Johnson, MEEP: A flexible free-software package for electromagnetic simulations by the FDTD method, *Comput. Phys. Commun.* **181**, 687 (2010).
- [36] S. Kako, *et al.*, A gallium nitride single-photon source operating at 200 K, *Nat. Mater.* **5**, 887 (2006).
- [37] E. B. Flagg, A. Muller, J. W. Robertson, S. Founta, D. G. Deppe, M. Xiao, W. Ma, G. J. Salamo, and C. K. Shih, Resonantly driven coherent oscillations in a solid-state quantum emitter, *Nat. Phys.* **5**, 203 (2009).
- [38] M. Schwartz, *et al.*, Fully on-chip single-photon Hanbury-Brown and Twiss experiment on a monolithic semiconductor-superconductor platform, *Nano Lett.* **18**, 6892 (2018).
- [39] A. Muller, *Resonance Fluorescence and Cavity Quantum Electrodynamics with Quantum Dots* (Ph.D. thesis, University of Texas at Austin, 2007).
- [40] G. Sallen, *et al.*, Subnanosecond spectral diffusion measurement using photon correlation, *Nat. Photon.* **4**, 696 (2010).
- [41] J. Johansen, B. Julsgaard, S. Stobbe, J. M. Hvam, and P. Lodahl, Probing long-lived dark excitons in self-assembled quantum dots, *Phys. Rev. B* **81**, 081304 (2010).
- [42] A. V. Kuhlmann, J. H. Prechtel, J. Houel, A. Ludwig, D. Reuter, A. D. Wieck, and R. J. Warburton, Transform-limited single photons from a single quantum dot, *Nat. Commun.* **6**, 8204 (2015).
- [43] R. Proux, M. Maragkou, E. Baudin, C. Voisin, P. Roussignol, and C. Diederichs, Measuring the Photon Coalescence Time Window in the Continuous-Wave Regime for Resonantly Driven Semiconductor Quantum Dots, *Phys. Rev. Lett.* **114**, 067401 (2015).
- [44] P. Tighineanu, C. L. Dreessen, C. Flindt, P. Lodahl, and A. S. Sørensen, Phonon Decoherence of Quantum Dots in Photonic Structures: Broadening of the Zero-Phonon Line and the Role of Dimensionality, *Phys. Rev. Lett.* **120**, 257401 (2018).
- [45] R. Lettow, Y. L. A. Rezus, A. Renn, G. Zumofen, E. Ikonen, S. Götzinger, and V. Sandoghdar, Quantum Interference of Tunably Indistinguishable Photons from Remote Organic Molecules, *Phys. Rev. Lett.* **104**, 123605 (2010).
- [46] M. J. Woolley, C. Lang, C. Eichler, A. Wallraff, and A. Blais, Signatures of Hong–Ou–Mandel interference at microwave frequencies, *New J. Phys.* **15**, 105025 (2013).
- [47] M. O. Scully and M. S. Zubairy, *Quantum Optics* (Cambridge University Press, Cambridge, 1997).
- [48] S. Gerber, *et al.*, Quantum interference from remotely trapped ions, *New J. Phys.* **11**, 013032 (2009).
- [49] J. Hansom, C. H. H. Schulte, C. Matthiesen, M. J. Stanley, and M. Atature, Frequency stabilization of the zero-phonon line of a quantum dot via phonon-assisted active feedback, *Appl. Phys. Lett.* **105**, 172107 (2014).
- [50] X. Zhou, P. Lodahl, and L. Midolo, In-plane resonant excitation of quantum dots in a dual-mode photonic-crystal waveguide with high  $\beta$ -factor, *Quantum Sci. Technol.* **7**, 025023 (2022).
- [51] A. Tiranov, *et al.*, Collective super- and subradiant dynamics between distant optical quantum emitters, *Science* **379**, 389 (2023).
- [52] C. Papon, *et al.*, Nanomechanical single-photon routing, *Optica* **6**, 524 (2019).
- [53] X. Zhou, *et al.*, On-chip nanomechanical filtering of quantum-dot single-photon sources, *Laser Photon. Rev.* **14**, 1900404 (2020).